J Mater Sci (2008) 43:1897–1909
DOI 10.1007/s10853-007-2369-0

A complete GTN model for prediction of ductile failure of pipe

S. Acharyya · S. Dhar

Received: 21 November 2006 / Accepted: 3 December 2007 / Published online: 31 January 2008

Abstract The micro mechanical model by Gurson–Tvergaard–Needleman is widely used for the prediction of ductile fracture. Some material properties (Gurson parameters) used as material input in this model for simulation are estimated experimentally from specimen level. In this article an attempt has been made to tune the values of some of these Gurson's parameters by comparing the simulated results with the experimental results in the specimen level (axisymmetric tensile bar and CT specimens). An elastic–plastic finite element code has been developed together with Gurson–Tvergaard–Needleman model for void nucleation and growth. The initial value of f_c is determined from Thomason's limit load model and then tuned on the basis of best prediction of the failure of one-dimensional tensile bar. Then the load versus load line displacement and J versus Δa results for CT specimen are generated with the same code and the value of f_n is tuned to match the simulated J versus Δa results with the experimental results. Lastly the same code and the Gurson's parameters obtained are used to simulate the load versus load point displacement and crack growth for pipe with circumferential crack under four point bending. The simulated results are compared with the experimental results to assess the applicability of the whole method. In the proposed material modelling, post-yielding phenomena and necking of the tensile bar are simulated accordingly and strain softening due to void nucleation and growth has been taken care of properly and drop in stress is implicitly simulated through a model. Incremental plasticity theory with arc length method is used for the nonlinear displacement control problem.

List of symbols

ϕ	Gurson plastic potential
σ_{ij}	Stress tensor of porous aggregate
σ_{eq}	Effective stress of porous aggregate
σ_{m}	Mean stress of porous aggregate
σ'_{ij}	Deviatoric stress tensor of porous aggregate
γ_{ij}	Deviatoric part of total strain
γ^{p}_{ij}	Deviatoric part of plastic strain
q_1, q_2, q_3	Gurson's parameters
G	Shear modulus
K	Bulk modulus/Hardening coefficient in stress–strain law
h	Hardening constant
σ_{c}	Current yield stress of matrix material
J	J Integral
ε_{ij}	Strain tensor
$\varepsilon^{\mathrm{p}}_{ij}$	Plastic strain tensor
$\varepsilon^{\mathrm{p}}_{\mathrm{eq}}$	Effective plastic strain
$\bar{\varepsilon}$	Mean strain
n	Hardening exponent of stress–strain law
$\bar{\varepsilon}^{\mathrm{p}}$	Mean plastic strain
$\{\dot{\varepsilon}^{\mathrm{e}}\}$	Elastic strain rate vector
$\{\dot{\varepsilon}^{\mathrm{p}}\}$	Plastic strain rate vector
f	Void volume fraction
$\dot{f}_{\mathrm{nu}}$	Void growth rate due to nucleation
$\dot{f}_{\mathrm{gr}}$	Void growth rate due to growth

Introduction

Classical theory of Von Mises for yielding of ductile material does not account for hydrostatic part of the stress

S. Acharyya (✉) · S. Dhar
Department of Mechanical Engineering, Jadavpur University, Kolkata 700032, India
e-mail: sanjib_acharyya@hotmail.com

components. But it has been observed [1–3] that yielding of ductile materials with second phase hard inclusions are connected to void nucleation, growth and finally coalescence of voids into micro cracks. The above phenomenon depends not only on effective stress measure (σ_e) but also on the hydrostatic part (σ_m) of the stress component. Among lot of plastic potential functions [4, 5], which take into account of the effects of hydrostatic part of the stress components and the void-volume fractions, Gurson model of plastic potential is widely used for ductile failure of materials like steel where second phase hard inclusions like (Fe_3C) are present. Needleman and Tvergaard [6] investigated the ductile crack growth based on Gurson model. They modelled the fracture as a natural outcome of deformation process due to possibility of complete loss of load carrying capacity due to large void growth. In CCP specimen, they found that the fracture occurs very near to the limit load. Cheng and Yiu [7] investigated the growth of a single cylindrical hole ahead of a blunt crack tip using large deformation FE analysis in TPB specimen with different pre-crack depths using Gurson model.

Decamp et al. [8] studied the effect of size and geometry on ductile fracture using Gurson model of notched bars in C-Mn steels. Ragab [9] in his work predicted the fracture strain for ductile material based on Gurson–Tvergaard yield function and compared with experimental results. Finally a closed form strain-based fracture criterion was suggested. Pineau [10] studied the scatter and size effect on ductile and brittle fracture using micro mechanical models. It is found that the ductility or the fracture toughness decrease with increasing size of the specimen. Lee and Zhang [11] used Gurson's mixed hardening plasticity model with stress and strain controlled nucleation in uniaxial compression of cylinders under sticking friction to study the effect of strain hardening, nucleation models, yield surface and geometry on the distribution and evolutions of stress, strain void fraction and coalescence.

Qiu and Weng [12] presented the analytic estimates for yield function of elastic–plastic material with nondilute distributions of parallel or randomly oriented ellipsoidal voids and found no significant resemblance with Gurson's prediction in the special case spheroidal cavity.

A complete Gurson model has been introduced by Zhang et al. [13] which is a combination of the modified Gurson model which deals with microvoid nucleation and growth, and a physical microvoid coalescence criterion based on the plastic limit load model by Thomason. Rakin et al. [14] analysed fracture initiation of low-alloyed ferritic steel using Gurson–Tvergaard–Needleman (GTN) model and also analysed transferability of micro mechanical parameters determined on specimens without initial crack to pre-cracked specimens. Pavankumar et al. [15] used the damage parameters in Gurson model for analysing notched tensile specimens, a C(T)25 specimen and for predicting the fracture resistance behaviour of a cracked pipe and obtained good match with experimental results.

In recent past, GTN model has been included for material modeling in finite element software like ADINA, ABAQUS, Marc. Though there are some limitations of this software to implement all the features of GTN model, many researchers have published a number of papers on ductile fracture based on GTN model using this standard software [16–18].

The present work aims at deriving the constitutive equations from Gurson model of plastic potential and using it in an elastic–plastic finite element code to predict the plastic deformation and failure of components of ductile materials. Resistance against yielding increases with the plastic strain due to strain hardening accompanied by strain softening due to void nucleation and growth which sheds load bearing capacity showing drop in effective stress and squeezing of the radius of the yield surface. Thus simultaneous hardening and softening have been appropriately modelled within the program. The FE code takes into account of large strain and deformation. Necking of tensile bar is simulated. The application of Gurson–Tvergaard–Needleman model for ductile fracture simulation requires several material properties known as Gurson parameters as input. These material parameters are measured experimentally. In most cases an estimate of the parameter is only possible instead of exact assessment. Therefore in this work, an attempt has been taken to tune the appropriate values of some of the parameters on the basis of matching between simulated and experimental results at specimen level. The value of critical void volume fraction f_c plays a significant role in the simulation as at this value of void volume fraction, the void growth process is accelerated leading to voids coalescence. In classical model by Gurson–Tvergaard–Needleman, the value of f_c is considered as material input but it is very difficult to determine the accurate value of f_c experimentally. In this work, initial value of f_c is estimated from Thomason limit load model and then the final value of f_c is tuned comparing the simulated values of load versus diametral contraction with the experimental one of the tensile bar. Using these values for Gurson parameters the load versus load line displacement and J versus crack growth results are generated for CT specimen of the same material. Then comparing these simulated results for CT specimen with the experimental results for the same, the value of another parameter f_n is tuned. This final set of Gurson parameters are used to predict the load versus load point displacement and load versus crack growth results for pipes with circumferential crack under four point bending and compared with the experimental results.

Formulation

The present work deals with Gurson model to predict ductile failure using the following expression for plastic potential as

$$\phi(\sigma_{ij},f,\sigma_y)=\frac{\bar{\sum}^2}{\sigma_y^2}+2q_1f\cosh\left(\frac{3q_2\sum_m}{2\sigma_y}\right)-1-q_3f^2=0 \tag{1}$$

Tvergaard found the values for these constants ($q_1=1.5$, $q_2=1$ and $q_3=q_1^2$) to match the predictions of the model with the numerical results of a periodic array of voids. $\bar{\sum}$ and $\sum_m$ are the effective and mean stresses of the porous aggregate and σ_y is the flow stress of the incompressible matrix.

In this model, the void nucleation is a continuous process. Accordingly it is represented as

$$\dot{f}_{\mathrm{nu}}=A\cdot\dot{\varepsilon}^{\mathrm{p}}_{\mathrm{eq}} \tag{2}$$

A is a function of plastic strain $\varepsilon^{\mathrm{p}}_{\mathrm{eq}}$ in some statistical sense.

Needleman [19] introduces a normal distribution for A as given below,

$$A=\frac{f_n}{S_n\sqrt{2\pi}}\exp\left\{-\frac{1}{2}\left(\frac{\varepsilon^{\mathrm{p}}_{\mathrm{eq}}-\varepsilon_n}{S_n}\right)\right\} \tag{3}$$

Here f_n is the void volume fraction of void nucleating particles and S_n is the standard deviation and ε_n is the mean nucleating strain.

Void growth law is derived from the plastic incompressibility of the matrix material. Thus,

$$\dot{f}_{\mathrm{gr}}=(1-f)\dot{\varepsilon}^{\mathrm{p}}_{\mathrm{kk}} \tag{4}$$

and

$$\dot{f}=\dot{f}_{\mathrm{nu}}+\dot{f}_{\mathrm{gr}} \tag{5}$$

The following plasticity rules are used in deriving constitutive equation:

(a) Flow rules,

$$\dot{\varepsilon}^{p}_{ij}=\lambda\frac{\partial\phi}{\partial\sigma_{ij}} \tag{6}$$

(b) Hardening rules

$$\dot{\varepsilon}^{\mathrm{p}}_{\mathrm{eq}}=\frac{\dot{\sigma}_e}{h} \tag{7}$$

(c) Plastic work rate,

$$\sigma_{ij}\dot{\varepsilon}^{\mathrm{p}}_{ij}=(1-f)\sigma_{\mathrm{e}}\dot{\varepsilon}^{\mathrm{p}}_{\mathrm{eq}} \tag{8}$$

From Eqs. 7 and 8 the following expressions are obtained

$$\dot{\sigma}_{\mathrm{e}}=\frac{h\sigma_{ij}\dot{\varepsilon}^{\mathrm{p}}_{ij}}{(1-f)\sigma_{\mathrm{e}}},\quad \dot{\varepsilon}^{\mathrm{p}}_{\mathrm{eq}}=\frac{\sigma_{ij}\dot{\varepsilon}^{\mathrm{p}}_{ij}}{(1-f)\sigma_{\mathrm{e}}} \tag{9}$$

Gurson potential ϕ (Eq. 1) can be expressed as a strain potential

$$g\left(\varepsilon_{ij},\varepsilon^{p}_{ij},\sigma_{\mathrm{e}},f\right)=\frac{3}{2\sigma_{\mathrm{e}}^2}\left\{(2G)^2\left(\gamma_{ij}-\gamma^{p}_{ij}\right)\left(\gamma_{ij}-\gamma^{p}_{ij}\right)\right\}+2fq_1\cosh\left\{q_2\frac{9K}{2\sigma_e}(\bar{\varepsilon}-\bar{\varepsilon}^{\mathrm{p}})\right\}-\left(1+q_3f^2\right) \tag{10}$$

where G is the shear modulus and K is the bulk modulus. γ_{ij} and γ^{p}_{ij} are the deviatoric part of the total strain and plastic strain, respectively. $\bar{\varepsilon}^{\mathrm{p}}$ and $\bar{\varepsilon}$ and the mean plastic strain and the mean strain, respectively.

For consistency,

$$\frac{\partial g}{\partial\varepsilon_{ij}}\dot{\varepsilon}_{ij}+\frac{\partial g}{\partial\varepsilon^{p}_{ij}}\dot{\varepsilon}^{\mathrm{p}}_{ij}+\frac{\partial g}{\partial\sigma_{\mathrm{e}}}\dot{\sigma}_{\mathrm{e}}+\frac{\partial g}{\partial f}\dot{f}=0. \tag{11}$$

The elastic plastic stress–strain relationship is given by the material matrix [D^{EP}] where,

$$\left[D^{\mathrm{EP}}\right]=[D]-[D]\cdot[M] \tag{12}$$

Here $[D]$ gives elasticity matrix and $[M]$ gives the relation between total strain rate and plastic strain rate which can be derived using Eqs. 3–9 in Eq. 10.

Strain softening model

It is evident from Gurson yield function that the yield surface squeezes with the growth of voids. Therefore, there is a competition between the expansion of yield surface due to strain hardening and contraction due to void growth. At a large void volume fraction, squeezing of the yield surface dominates indicating the loss of load bearing capacity of the material point. The phenomenon is termed here as strain softening. Therefore Gurson model evolves itself the crack growth criteria by loosing the load bearing capacity of the element. It is thus inherent within the yield function. No external criterion for crack growth is required.

The yield function ϕ can be written as

$$\phi(\sigma,H,f)=\phi(p,q,H,f)=0 \tag{13}$$

σ is the current yield stress and H is the hardening function and f is an internal variable (11). Here it stands for void volume fraction as in Gurson model.

The hardening function H is given as,

$$\mathrm{d}H=h(\varepsilon^{\mathrm{p}},p,q,H,f) \tag{14}$$

Here p is the hydrostatic pressure and q is the Von Mises stress.

Incremental change for stress (σ), strain (ε), void volume fraction (f) and hardening (H) can be calculated at the nth iterative stage by the following formulations

$$\sigma_{n+1} = \sigma_n + \Delta\sigma_{n+1} \tag{15}$$

elastic increment of stress,

$$\Delta\sigma^T_{n+1} = [D]^{\mathrm{e}} \mathrm{d}\varepsilon^{n+1}, \tag{16}$$

where, $[D]^{\mathrm{e}}$ is elastic stress–strain matrix.

Effective increment of stress considering elastic increment and plastic return,

$$\Delta\sigma_{n+1} = \Delta\sigma^T_{n+1} - [D]^{\mathrm{e}} \mathrm{d}\varepsilon^p_{n+1} \tag{17}$$

As per associated flow rule,

$$\mathrm{d}\varepsilon^p_{n+1} = \lambda \left(\frac{\partial\phi}{\partial\sigma}\right)_n, \tag{18}$$

$$\phi_{n+1} = \phi(P_{n+1}, q_{n+1}, H_{n+1}, f_{n+1}) = 0 \tag{19}$$

Now total strain increment $\mathrm{d}\varepsilon^p_{n+1}$ can be split into volumetric part and deviatoric part as

$$\mathrm{d}\varepsilon^p_{n+1} = \mathrm{d}\varepsilon^p_v + \mathrm{d}\varepsilon^p_D = \lambda\left[-\left(\frac{\partial\phi}{\partial p}\right)_n \frac{1}{3}\delta_{ij} + \left(\frac{\partial\phi}{\partial q}\right)_n \frac{3}{2}\frac{\sigma'_{ij}}{q_n}\right] \tag{20}$$

Then,

$$\Delta\sigma_{n+1} = \Delta\sigma^T_{n+1} - K\Delta\varepsilon^p_m \cdot I - 3G\Delta\varepsilon^p_q \frac{\sigma'_{ij}}{q_n} \tag{21}$$

K and G stands for bulk modulus and modulus of rigidity respectively and I stands for unit matrix.

$$p_{n+1} = p^T_{n+1} + K \cdot \Delta\varepsilon^p_m$$

$$\sigma'_{ij\,n+1} = \sigma'_{ij\,n+1} - 3G\Delta\varepsilon^p_q \frac{\sigma'_{ij}}{q_n} \tag{22}$$

$$\sigma_{ij\,n+1} = -p_{n+1}\delta_{ij} + \sigma'_{ij\,n+1} \tag{23}$$

The above softening model is incorporated in Gurson model within Newton–Raphson [20, 21] iteration cycle for satisfying the equilibrium equations. The Eq. 19 is satisfied iteratively using the current value of P_{n+1}, q_{n+1}, H_{n+1} and f_{n+1}. The error arising out of Eq. 19 is used to modify the plastic strain rate $\mathrm{d}\varepsilon^{\mathrm{p}}$, $\mathrm{d}\varepsilon^{\mathrm{p}}_{\mathrm{m}}$ and $\mathrm{d}\varepsilon^{\mathrm{p}}_q$. This modifies the values of P_{n+1}, q_{n+1}, σ_{n+1}, etc. The process repeats unless $\Delta\phi_{n+1}$ becomes 1.0×10^{-3}.

Finite element formulation

The above formulation for constitutive equations is implemented in a elastic–plastic finite element code developed in-house together with the strain softening model discussed earlier. The FE code is capable to consider different material models like Gurson model, Rousellier model, Thomason model and Lamaitre model. Material nonlinearity as well as geometric nonlinearity with large strain are considered. Stress–strain relation can be given as functional form. The algorithm is based on updated Lagrangian method and discussed in Ref. [22]. Newton–Raphson iteration scheme along with arc length method has been used as numerical schemes for searching equilibrium solutions and to converge in neighbourhood of the critical point. Incremental plasticity with arc length method is used to solve the displacement control problem. Matching of yield surface is ensured even within each iteration of Newton–Raphson iteration while searching for equilibrium which enhances the convergence. Results can be generated both by load control and displacement control. For displacement control, the incremental step size can be self-adjusted with the change in stiffness of the load–displacement curve. The first specimen is an axisymmetric tensile bar. Necking is simulated by introducing geometric imperfections of 0.001 mm in radial dimension of the specimen. Unloading is indicated by the fall of effective stress value from its previous value which is considered as the current yield stress of the material. A (2×2) reduced Gauss point integration scheme is taken for eight-noded isoparametric elements. Stress, strain, void volume fraction and other continuum parameters are computed at the Gauss points. True stress is calculated by dividing the load by the current cross-sectional area at the middle of the specimen. True strain is obtained by $2\ln(d_0/d_i)$, where d_0 is the initial diameter and d_{i} is the current diameter of the specimen respectively, at the middle of the specimen. The results obtained from the FE program is validated against the experimental results obtained from Bhabha Atomic Research Centre, India.

The crack growth in a plane strain CT specimen is simulated using same code mentioned above. As void volume fraction f increases, the load bearing capacity of the elements gradually decreases which is captured in FE program by matching Yield surface each time after f is updated. Finally, the element loses most of its load bearing capacity (98%) when f reaches f_{f}. Thus the crack propagation is inherently simulated. Load versus load line displacement for the CT specimen with growing crack is computed and compared with the experimental results obtained from Bhabha Atomic Research Centre, India. Finally J–R curve is obtained and compared with the experimental data. All the problems are treated as displacement-controlled.

Failure criterion

Gurson model does not give any failure criterion. The void growth law shows that the void will grow continuously with strain. In real sense, the void growth law is applicable upto a critical value of the void, f_{c}. After attending the

value of f_c, the void growth is an accelerated process which will lead to final failure. Thus one can write Gurson potential (Eq. 1) as

$$\phi = \frac{\sum^2}{\sigma_e^2} + 2q_1 f^* \cosh\left\{3q_2 \frac{\sum_m}{2\sigma_e}\right\} - q_3 f^{*2} - 1 = 0$$

with $f^* = f$ for $f \le f_c$

$$= f_c + \frac{f_u^* - f_c}{f_f - f_c}(f - f_c) \quad \text{for } f > f_c \tag{24}$$

The material point loses its load bearing capacity fully when $f = f_f$ or $f^* = f_u^*$, where, $f_u^* = 1/q_1$.

The above value of f_u^* which shows 100% squeezing of yield surface is difficult to achieve in a numerical scheme. The value of $f_u^* = 0.58$ which shows 98% squeezing of yield surface has been achieved in this computation work. Thus, as strain increases the value of 'f' increases upto 'f_c' at a certain rate controlled by void growth and void nucleation rate. At this point the crack initiates which enhances the void growth phenomenon. This point is identifiable in load versus diametral contraction curve of a tensile bar. At this point, the stiffness of the load versus diametral contraction curve falls remarkably. After f reaches 'f_c', the value f increases at higher rate and becomes f_f for which the radius of yield surface i.e. the load bearing capacity falls to almost nil. This situation is considered as failure. This point is also observed in load versus diametral contraction curve of a tensile bar.

Evaluation of J-Δa curve

The J integral [23] for elasto-plastic crack growth in CT specimen is split into two parts.

Thus,

$$J = J_e + J_{pl}$$

Here J_e stands for elastic part of J integral.

For plane strain J_e is calculated as,

$$J_e = \frac{K_I^2(1-\gamma^2)}{E} \tag{25}$$

where, K_I is the mode I stress intensity factor which is calculated by standard formula for CT specimen. γ stands for Poisson's ratio.

The plastic part of J integral 'J_{pl} ' is calculated from the area under the load–load point displacement curve. Thus,

$$J_{pl} = \frac{\eta \cdot A_{pl}}{B \cdot b} \tag{26}$$

Here A_{pl} is the plastic part of the area under the load versus load point displacement curve and B is the width of the specimen and b is the ligament length η is standard Eta factor for CT specimen.

Material

The material used is 22NiMoCr37. The mechanical and metallurgical properties of the material is collected from Bhabha Atomic Research Centre, India and are given in Tables 1, 2, 3, and 4. The stress–strain data are fitted with a power law-hardening curve.

(i) 22NiMoCr37 (Pressure vessel steel)
(ii) SA 333 Gr-6 (Carbon Steel for primary heat transport pipes)

The first attempt is made with an axisymmetric tensile specimen of material 22NiMoCr37 for which load versus diametral contraction curve and stress–strain data are available from Bhabha Atomic Research Center, India.

The basic objectives of this study are:

(a) To generate and compare the FE simulated failure results based on GTN model with the experimental results.
(b) To determine the value of critical void–volume fraction (f_c) from physical microvoid coalescence criterion based on the plastic limit load model by Thomason and to tune the value of f_c for the best matching with the experimental load deflection curve.
(c) The strain softening behaviour is compared with stress–strain–void results.
(d) The parametric study of different set of values of q_1, q_2, q_3 with load–deflection and void growth curve.

Results and discussion of axi-symmetry tensile bar

The first set of results are generated with the following values using GTN model taking the values of Gurson parameters as listed in Table 2 for the material 22NiMoCr37.

$q_1 = 1.5$, $q_2 = 1.0$, $q_3 = 2.25$, $f_c = 0.028$.

Figure 1 shows load versus diametral contraction curve for the tensile specimen. At point P, there is a sharp change in the slope and drastic fall in load showing the initiation of failure process.

Figure 2 shows strain-softening results at the middle of the tensile bar. At a strain level of 75% equivalent stress (σ_{eq}) starts falling. Figure 3 also shows that profuse void growth occurs after a strain level of 75%. From the curves strain softening behaviour at the accelerated void growth is apparent.

Table 1 Mechanical properties of 22NiMoCr37

Young's Modulus E (GPa)	Poisson's ratio	$\sigma_{y\cdot p}$ (Mpa)	σ_{ult} (Mpa)	ε_{ult}	$\sigma = K \cdot \varepsilon^{n}$	
					K (MPa)	n
210	0.3	400	728	0.13	950	0.13

Table 2 Gurson parameters of 22NiMoCr37

Parameters	f_o	f_n	ε_n	S_n	f_c	f_f	q_1	q_2	q_3
Values	0.0001	0.008	0.25	0.10	0.028	0.18	1.5	1.0	2.25

Table 3 Gurson parameters of SA 333 Gr-6 Carbon Steel

Parameters	f_o	f_n	ε_n	S_n	f_c	f_f	q_1	q_2	q_3
Values	0.0001	0.005	0.3	0.10	0.03	0.18	1.5	1.0	2.25

Parametric study with q_1, q_2 and q_3

The load versus diametral contraction and void versus strain curves for different set of q_1, q_2 and q_3 are shown in Figs. 4 and 5. From the figures, it is observed that the best matching with the experimental results are obtained for the values of $q_1 = 1.25$, $q_2 = 1$, $q_3 = 2.25$ as proposed by Tvergaard.

A complete Gurson model approach

In the Gurson–Tvergaard–Needleman (GTN) model, only the void nucleation and void growth are simulated and is assumed that coalescence occurs when a critical void volume fraction f_c has been reached. In the present study, a physical microvoid coalescence criterion based on the plastic limit load model by Thomason [24] has been used to determine initial value of f_c and then the final value of f_c is tuned comparing the simulated results with experimental results. Thus f_c is not a predetermined experimental quantity rather it is determined from Thomason plastic limit load model for coalescence criteria. The plastic limit load criterion for coalescence as derived from Thomason model for a general 3D problem at a specific material point is given as:

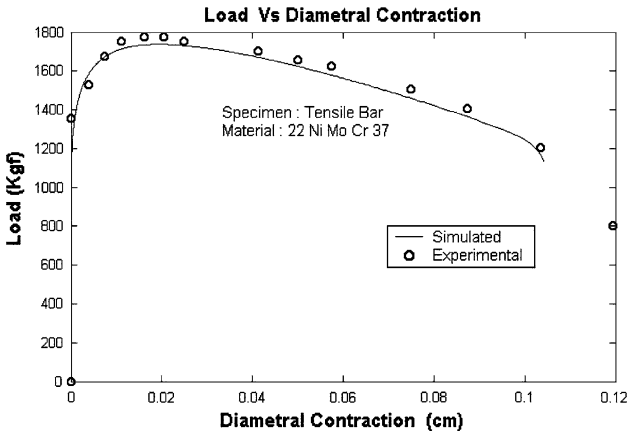

Fig. 1 Load versus diametral contraction of tensile bar

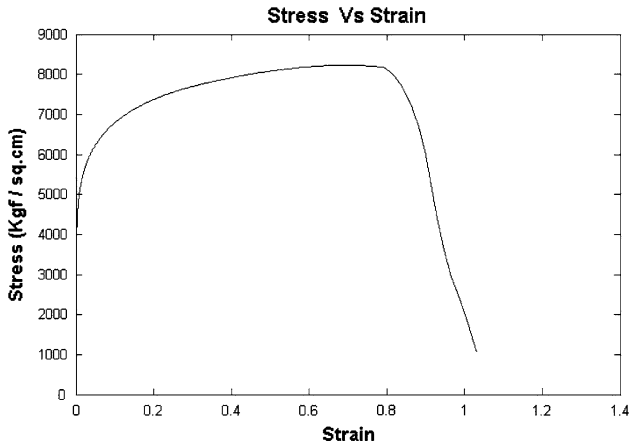

Fig. 2 Stress versus strain of tensile bar

$$\frac{\sigma_1}{\sigma} = \left(\alpha\left(\frac{1}{r} - 1\right)^2 + \frac{\beta}{\sqrt{r}}\right)\left(1 - \pi r^2\right) \quad r = \frac{\sqrt[3]{\left(\frac{3f}{4\pi}\right)}e^{\varepsilon_1+\varepsilon_2+\varepsilon_3}}{\left(\sqrt{e^{\varepsilon_2+\varepsilon_3}}\right)} \tag{27}$$

where σ_1 is the maximum principal stress, r is the void space ratio and ε_1 is the maximum principal strain and ε_2, ε_3 are the other two principal strains.

Table 4 Mechanical properties of SA 333 Gr-Carbon Steel

Young's Modulus E (MPa)	Poisson's ratio	$\sigma_{y\cdot p}$ (MPa)	σ_{ult} (MPa)	ε_{ult}	$\sigma = K \cdot \varepsilon^{n}$	
					K (MPa)	n
203000	0.3	312	728	0.13	677.05	0.159

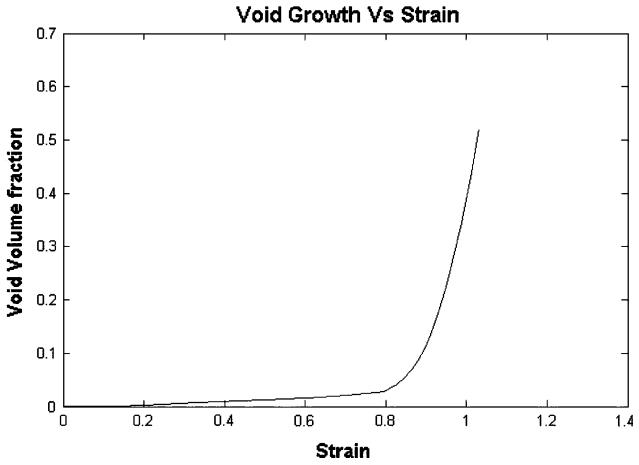

Fig. 3 Void volume fraction versus strain of tensile bar

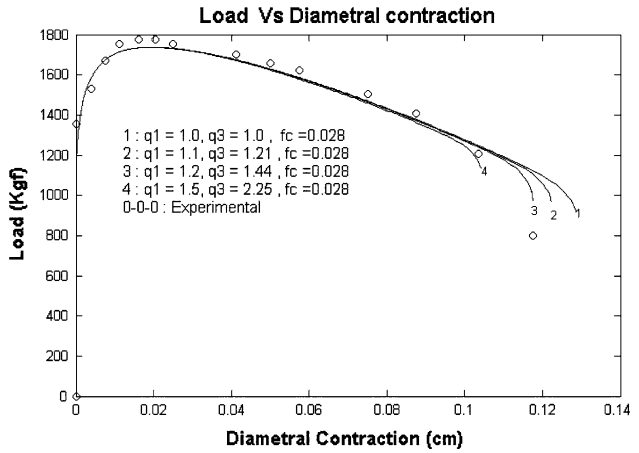

Fig. 4 Load versus diametral contraction of tensile bar with different q_1, q_2, q_3

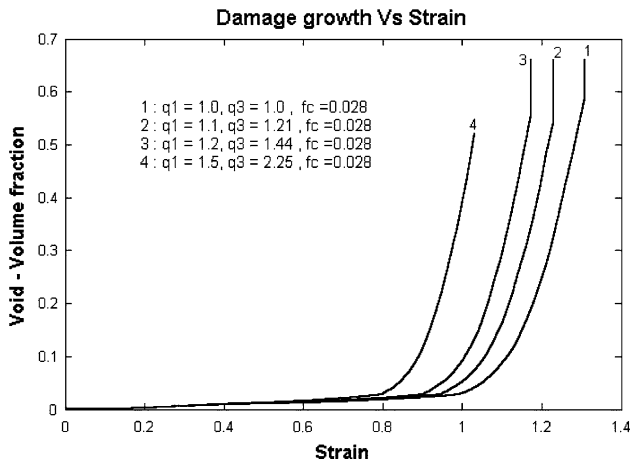

Fig. 5 Void volume fraction versus strain of tensile bar with different q_1, q_2, q_3

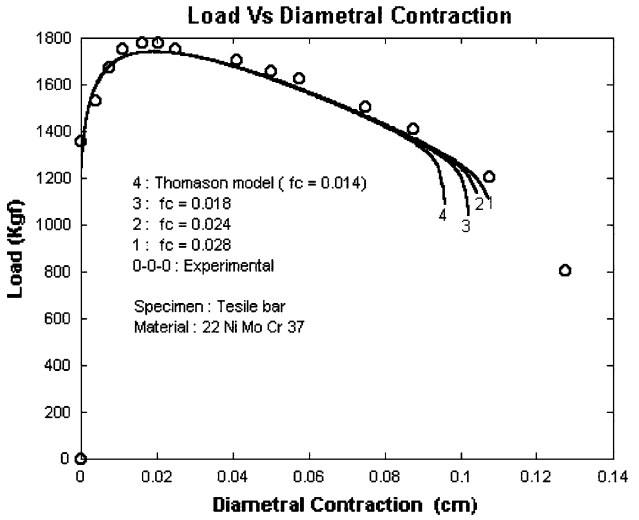

Fig. 6 Load versus diametral contraction of tensile bar with different f_c

$\alpha = 0.1$, $\beta = 1.2$ are two constants fitted by Thomason. The same equation can be applied for plane strain by making $\varepsilon_3 = 0$.

Using Thomason coalescence model 'f_c' is found to be 0.014. After tuning, the simulated results show that the best matching is obtained with 'f_c' as 0.028 as apparent from Fig. 6. The void versus strain results for different 'f_c' are shown in the Fig. 7. The effect of q_1, q_2, q_3 and f_c on void versus strain curve is more prominent than that on load versus displacement. This is because the 'f' is modified directly at 'f_c' and the effect of this change in the load bearing capacity of the specimen is captured through the squeezing of yield surface.

After the axisymmetric study, the optimal values for f_c and q_1, q_2 and q_3 have been settled. Now these values are used to generate simulated FE results for CT specimen

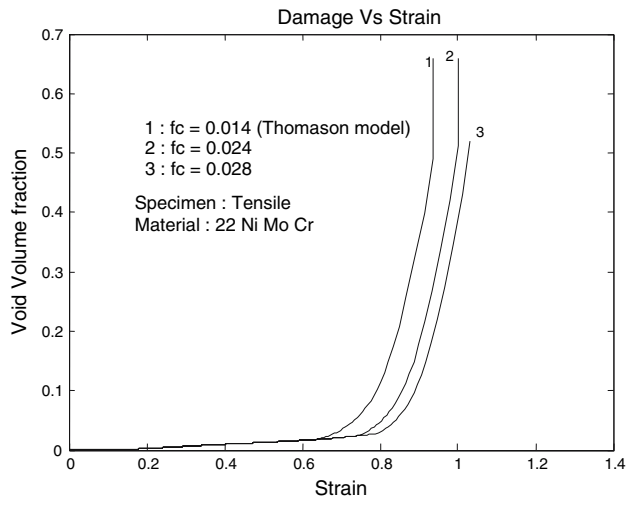

Fig. 7 Void volume fraction versus strain of tensile bar with different f_c

using the same GTN model. The simulated results obtained are compared with the experimental results. Load versus load point Displacement (LLD) have been generated for both the plane strain and 3D cases. '*J*' Integral at different crack length also has been calculated for plane strain case. The parametric study with the values of f_0 and f_n on J-Δa curve have been explored.

Results and discussion of CT specimen

Figure 8 shows load versus load point displacement of CT specimen. For crack tip element size (0.2×0.2 mm^2), the matching of simulated results with experiment is better.

Figure 9 shows simulated J–R curve as compared to experimental results. For crack tip mesh size (0.1×0.1 mm^2), *J* values are much lower than experimental values. For mesh sizes (0.2×0.2 mm^2), the matching is somehow closer to experimental values. The slope of the J-Δa curve is closely matches with the experimental data but initiation value (J_I) for simulated result is much lower than that of experimental value.

Parametric study with f_0 and f_n

In the Fig. 9, it is observed that though the slope of the J-Δa curve closely matches with the experimental data but initiation value (J_I) for simulated result is much lower than that of experimental value. The value of the f_0 can be determined experimentally easily and is much reliable but the value of f_n is very difficult to determine and only an approximate value can be determined. Therefore different set of values of f_0 and f_n are used and the effect on the J-Δa curve and Load versus LLD curve for CT specimen are studied (Figs. 10 and 11). The value of f_0 is kept fixed as

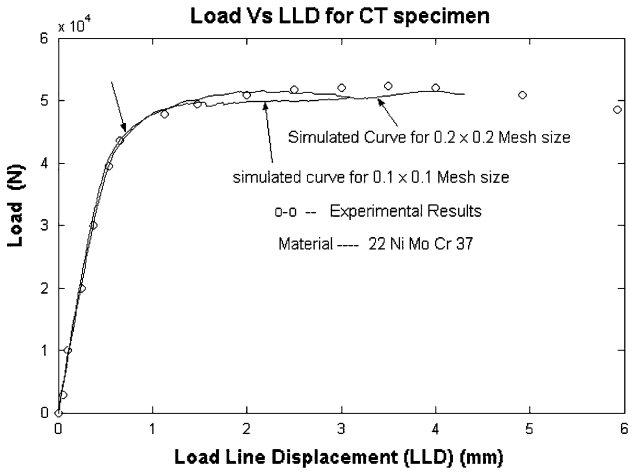

Fig. 8 Load versus LLD of CT specimen

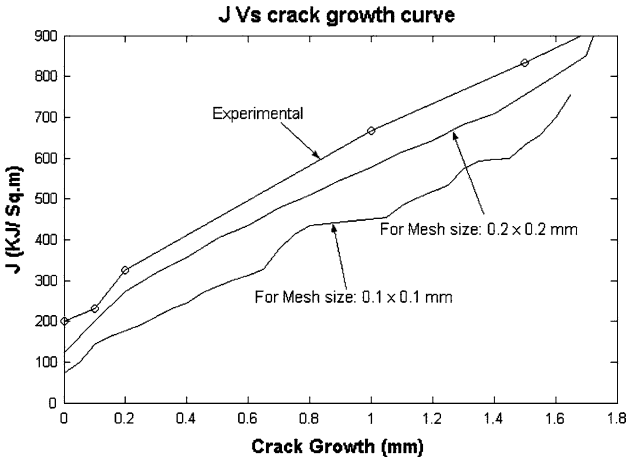

Fig. 9 *J* Integral versus crack growth of CT specimen

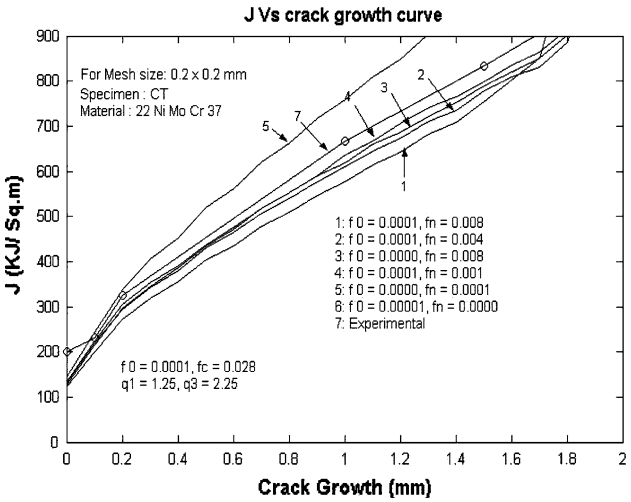

Fig. 10 *J* Integral versus crack growth of CT specimen with different combinations of f_c and f_n

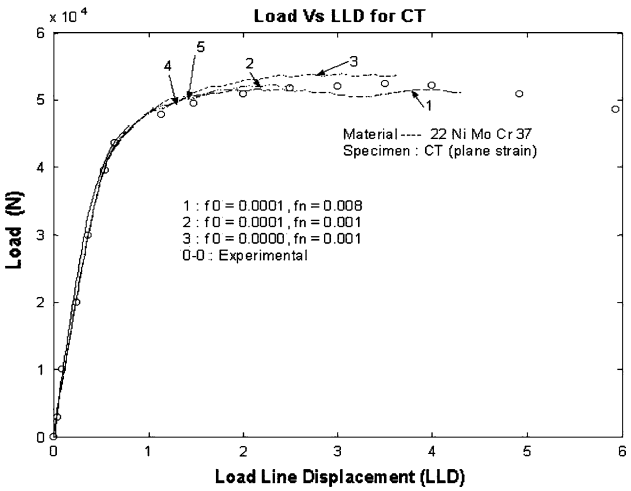

Fig. 11 Load versus LLD of Ct specimen with different combinations of f_c and f_n

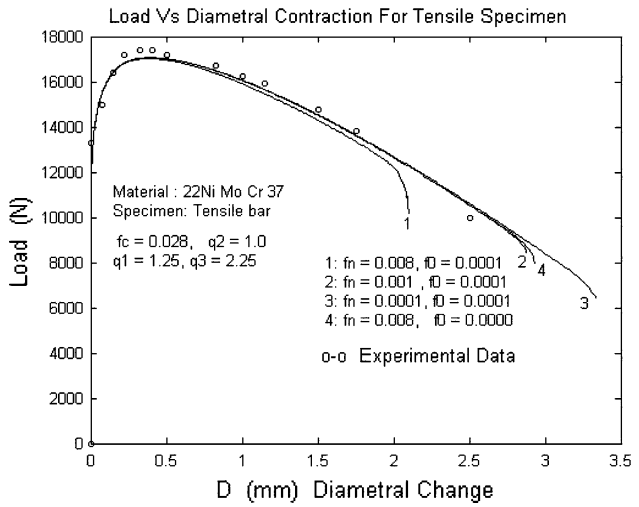

Fig. 12 Load versus diametral contraction of tensile bar with different f_0 and f_n

obtained experimentally (0.0001) and the best matching between the simulated J-Δa curve with the experimental curve is found for the value of $f_n = 0.001$. The Load versus LLD curves for tensile specimen with this set is also verified against the experimental curve (Fig. 12) and no significant deviation is found. The values of f_c and q_1, q_2, q_3 were determined from the results of tensile bar and now from the CT results the appropriate value of f_n is found out. This leads to a scheme to finalise the Gurson parameters of a material in a methodical approach.

From the above study with the results on CT specimen, the following findings are made:

(1) The prediction of load versus load point displacement curve with the values of Gurson parameters obtained from experimental results and simulated study on Tensile specimen matches well with experimental curve.
(2) The J-Δ*a* curve for CT specimen can be appropriated with the experimental results by proper tuning of f_n.
(3) The final values of the different Gurson parameters finalised on the basis of tensile and CT specimen results are again applied for predicting results for tensile specimen and the matching of the prediction with the experimental results is verified once again.
(4) Thus a systematic scheme for finalisation of the values of Gurson parameters obtained experimentally can be suggested as:
   (i) To start with, the experimental values of the Gurson parameters and to predict load versus diametrical contraction using Thomason Plastic Limit load model for finding the lower limit of f_c.
   (ii) After tuning, the proper value of f_c is determined by comparing the simulated load versus diametrical contraction results with the experimental results for tensile specimen.
   (iii) Then the value of f_n is found by comparing the simulated J-Δ*a* curve with the experimental results.

Thus a final set of the values of Gurson parameters of the material can be obtained which can be applied for failure prediction of component like pipe.

But the final objective of this work is to develop a finite element simulation code to predict Load carrying capacity of pipes with crack. The experimental failure data for the pipes with circumferential crack under four point bending are available for the material *SA 333 Gr-6 Carbon Steel*. Therefore, the values of the Gurson parameters for this material are to be finalised on the basis of tensile and CT specimen test results. To achieve this objective, some experiments are done with tensile and CT specimens at the National Metallurgical Laboratory, Jamshedpur, India. The stress–strain, load versus diametral contraction data for axisymmetric tensile specimen and load versus load point displacement and '*J*' Integral versus crack growth data for several CT specimens are generated. An approximate experimental estimate of Gurson parameters are also available.

These material parameters are used to simulate FE results for the tensile specimen and CT specimens of material SA 333 Gr-6 Carbon Steel. After the same type of analysis and parametric study as it was done for 22Ni-MoCr37 the final values of the Gurson parameters are settled for *SA 333 Gr-6 Carbon Steel* material. Those values are listed in Tables 5 and 6.

Results and discussions on pipe

The values for the different Guson parameters are experimentally determined and then the values of f_c and f_n are properly tuned on the basis of the tensile and CT specimen results for the material SA-333 Gr-6 Carbon steel (as discussed in Sect. "Failure criterion"). Now these values for the

Table 5 Mechanical properties of SA 333 Gr-6 Carbon Steel

Young's Modulus E (Gpa)	Poisson's ratio	$\sigma_{y \cdot p}$ (Mpa)	σ_{ult} (Mpa)	ε_{ult}	$\sigma = K \cdot \varepsilon^n$	
					K (MPa)	n
203	0.3	245	511	0.151	673.6	0.1434

Table 6 Gurson parameters of SA 333 Gr-6 Carbon Steel

Parameters	f_o	f_n	ε_n	S_n	f_c	f_f	q_1	q_2	q_3
Values	0.0001	0.004	0.3	0.10	0.03	0.18	1.5	1.0	2.25

Gurson parameters are used for the analysis of Pipe with circumferential crack under four point bending load (Table 6).

The experimental data for Load versus Load point displacement(LLD) and load versus crack growth for pipes are obtained from BARC, India.

Geometry and size of the Pipe

Test specimen

Test specimen is a straight pipe of SA 333 Gr-6 Carbon Steel material with circumferential through wall crack at the middle of the pipe length (Fig. 13). The details of the loading and supporting arrangement are shown in the Fig. 13 and also listed in Table 7. The notched test specimens are fatigue pre-cracked by a sinusoidal cyclic load (10% of collapse load) before the experiment.

FE model for simulation of pipe in four point bending

The actual loading and supporting arrangement for the pipe under four point bending test is shown Fig. 14a. The large size of the specimen and requirement of fine meshing at the crack tip makes Element computation highly time-consuming. Therefore, an alternative finite element modelling of the same test is proposed which makes the problem convenient for finite element computation.

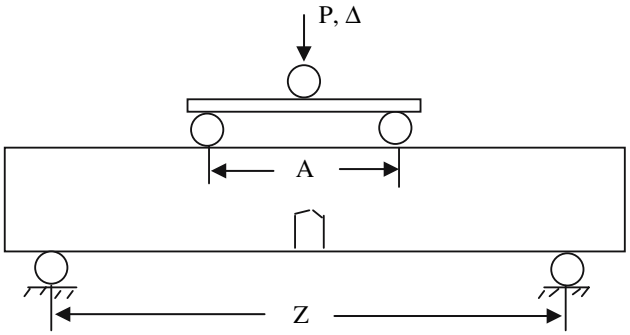

Fig. 13 Geometry of the pipe test

As the crack face is loaded with constant bending moment in four point bending test, it is better to load that portion with constant bending moment and to compute moment (M) and slope (ϕ) from FE results (Fig. 14b).

Since we are using 3D FE analysis, the moment is simulated with distributed couples at the end faces (Fig. 15). The equal and opposite forces for the couple are distributed according to the stress distribution over the cross section under pure bending i.e. in proportion to distance from the neutral axis. Figure 16 shows such a distribution. ϕ is calculated from the rotation of the end faces (Fig. 15). Thus moment M versus ϕ results are obtained [25] (Fig. 17).

Calculation of load and load point displacement

Formulation of load and displacement from moment and end rotation

For the convenience of finite element implementation of the pipe under FPB, the central portion of the pipe is modelled under constant bending moment and the results for moment versus end rotation (M$-\phi$) are computed by the FE programme. But the experimental results are available for load versus load point displacement. Therefore, the computed M$-\phi$ results has to be converted to load (F) versus load point displacement (Δ). This is done by separating the cracked and non-cracked displacements following the principle described by Zahoor [25] as discussed below.

Total displacement Δ is contributed by cracked displacement Δ_c (additional displacement that occurs due to the presence of the crack) and the non crack displacement Δ_{nc} (displacement that occurs even in the absence of crack)

$$\Delta = \Delta_{nc} + \Delta_c$$

Δ_{nc} is considered here to be elastic only.

For bending moment 'M', the equivalent force 'F' at the load point is calculated as,

$$M = F \cdot (Z - L)/4.0 \qquad (28)$$

(Z and L are shown in Fig. 13)

Table 7 Details of the pipe test arrangement under FPB

Sl. no	Test. no	Outer diameter (mm)	Wall thickness (mm)	Outer span (Z) (mm)	Inner span (A) (mm)	Crack angle (°)
1	SPBMTWC8-1	219	15.15	4000	1480	65.6
2	SPBMTWC8-2	219	15.15	4000	1480	110

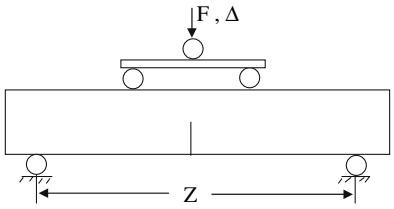

(a) Test set up for three point bending of pipe

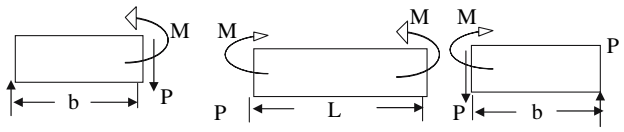

(b) Loading simulation of three point bending load in pipe

Fig. 14 (**a**) Test set up for three point bending of pipe. (**b**) Loading simulation of three point bending load in pipe

Fig. 15 End rotation due to bending of pipe

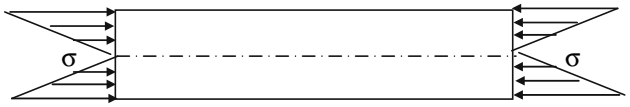

Fig. 16 Triangular distribution of stress

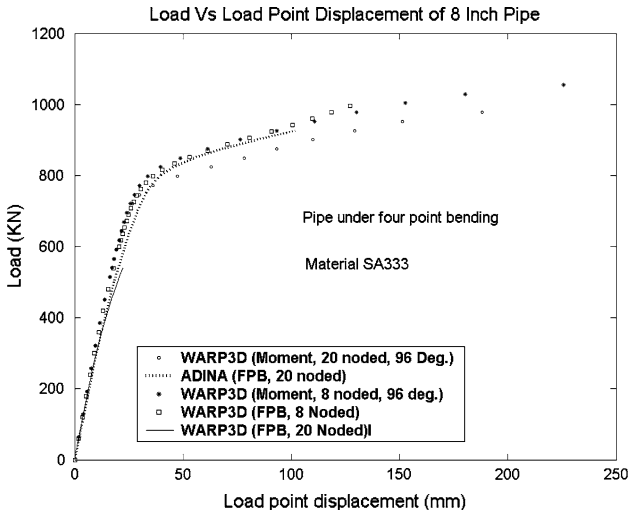

Fig. 17 Simulated results of four point bend pipe test using different software and FE models

The elastic energy stored in the beam (Fig. 14b) is contributed by the central part which is loaded under constant bending moment and the two end parts which are loaded as cantilever beams.

Thus,

$$U_{el} = \frac{M^2 L}{2EI} + 2\frac{P^2 (b)^3}{6EI} \tag{29}$$

where $P = F/2$ and $b = Z - L/2$.

This elastic energy is the elastic work input at the load point.

Thus,

$$\frac{1}{2} F \cdot \Delta_{\mathrm{nc}} = U_{\mathrm{el}}$$

Therefore Δ_{nc} is obtained.

Again the total end rotation at the cracked face consists of two parts namely the noncrack and crack portion.

Thus, $\phi = \phi_{\mathrm{nc}} + \phi_{\mathrm{c}}$.

Here also the ϕ_{nc} is elastic only.

ϕ_{nc} is obtained as,

$$\phi_{\mathrm{nc}} = \frac{M \cdot L}{E \cdot I} \tag{30}$$

As total ϕ is computed by FE calculation, ϕ_{c} is obtained as

$$\phi_{\mathrm{c}} = \phi - \phi_{\mathrm{nc}}$$

Δ_{c} is calculated from ϕ_{c} according to Zahoor [25]

Thus,

$$F \cdot \Delta_{\mathrm{cp}} = M \cdot \phi_{\mathrm{cp}} \tag{31}$$

If the elastic component for cracked displacement, Δ_{c} and cracked bending angle, ϕ_{c} are neglected.

Now the total displacement Δ at the load point is obtained as

$$\Delta = \Delta_{\mathrm{c}} + \Delta_{\mathrm{nc}}$$

Thus following the above steps the load versus load point displacement for a pipe under four point bending can be calculated from the FE computed moment versus end rotation data.

From the above figure, it is apparent that the load versus load point displacement curve computed directly or computed from M versus ϕ method using the finite element WARP3D package matches very well for eight noded and also for 20 noded elements. The result also shows good matching with the results computed using finite element package ADINA. Therefore, it can be concluded now that the load versus load point displacement for a cracked pipe under four point bending can be calculated by modelling the central part under constant bending moment and then calculating the total displacement using the formulae discussed above. The validation of the proposed FE model is done with the standard packages which are well tested for

finite element computations. Hence, this method can be used for calculating the load versus load point displacement for a cracked pipe under four point bending with growing crack using GTN model.

Detail of the pipe for the application of GTN model

See Table 8.

FE simulation results of pipe with growing crack using GTN model

The FE modelling of pipe under four point bending proposed in the previous section has been validated through standard software and also with the in-house FE code. The present work is with the objective to simulate load versus load point displacement of pipe with growing circumferential crack under four point bending. The FE code using GTN material model developed and tested through tensile and CT specimen results is capable of simulating crack growth phenomenon. The FE simulated results for moment versus end rotation for pipe with growing crack having initial circumferential crack of 110° are generated using the FE code. Then using the formulae described in Sect. "Formulation of load and displacement from moment and end rotation", load versus load point displacement results are calculated from moment versus end rotation (M versus ϕ) results.

The results are plotted in the Figs. 18 and 19 along with the experimental results.

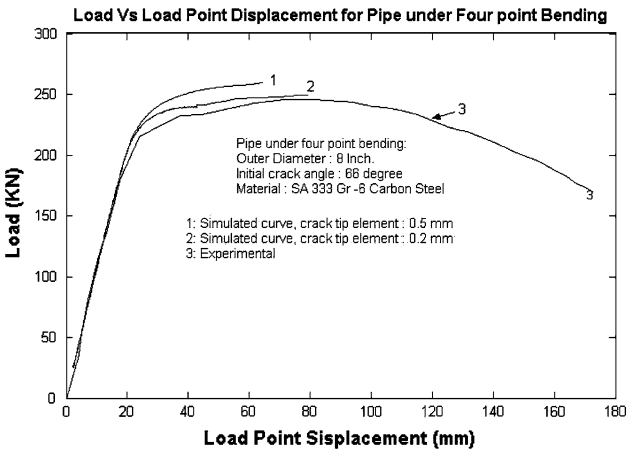

Fig. 18 Load versus load point displacement of pipe using Gurson model and experiment

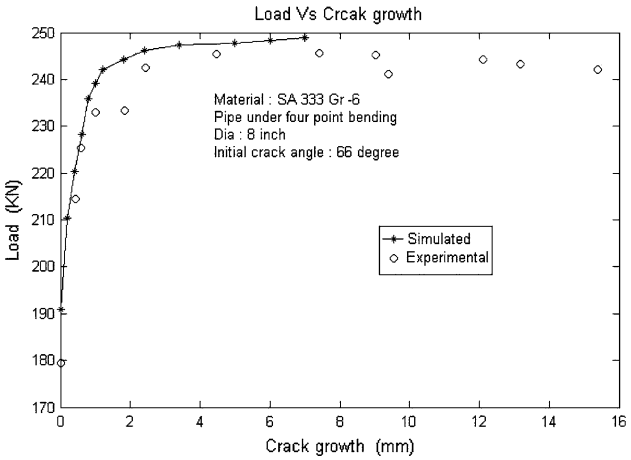

Fig. 19 Load versus crack growth of pipe using Gurson model and experiment

Observations and conclusions

The load versus load point displacement of a pipe with circumferential crack is computed using GTN model for growing crack. The results are plotted in Fig. 18. The simulated results are generated for two crack tip element sizes. The first choice of elements just ahead the crack tip and just behind are of 0.5×0.5 mm^2 and the results show a little higher stiffness compared to experimental results and also higher resistance against crack growth because of larger elements ahead of the crack tip. Then the crack front is finely meshed to 0.2×0.2 mm^2 which is twice the size of l_c. Then the results exhibit better matching. Due to high computation time, results are taken up to the maximum load. Figure 19 shows the simulated and experimental load versus crack growth data. The crack growth is calculated from the number of element losing load-bearing capacity due to strain softening and for which yield surface is squeezed up to 95%. The crack growth data also exhibits a little higher crack growth resistance which is also apparent from load versus displacement curve.

Thus the GTN model is applied to predict the load bearing capacity of a pipe under four point bending with crack growth. The Gurson parameters are found out from tensile experiment and then also tuned based on

Table 8 Details of the pipe under FPB using GTN model

Sl. no	Test. no	Outer diameter (mm)	Wall thickness (mm)	Outer span (Z) (mm)	Inner span (A) (mm)	Crack angle (°)
1	SPBMTWC8-2	219	15.15	4000	1480	110

experimental results at specimen level. The Gurson parameters thus finalised can be used well for components. From the simulated results, it can be concluded that the code and methodology developed using GTN model is capable of predicting ductile fracture at the component level. The material data used for the simulation of pipe are all extracted and determined at the specimen (tensile & CT) level. For the crack growth of pipe, no specific crack growth property of pipe is required. The advantage of this methodology over *J* Integral-based method of modelling ductile fracture is that the material property based on *J* integral is transferable from specimen to component level. Hence, for each component, experiment is required to determine fracture parameters which can be avoided while using the GTN model. The approximations in the values of Gurson parameters determined from metallurgical inspection can also be appropriated based on experimental results at specimen level. Once appropriated, these values can be used for any component.

Even for a component for which J-Δa data is given the simulation of load, displacement and crack growth using J_i and J-Δa data is a stepwise discrete process. It requires conventional nodal release or element extinction technique to be forced externally and hence possess numerical problems. Whereas in FE analysis with GTN model, the crack growth is a continuous process and a natural outcome of material response. Hence, all the parameters are updated continuously and the numerical stability is better.

References

1. Mackenzie JHAC, Hancock JW, Brown DK (1977) Eng Fract Mech 9:167
2. Gurland J (1972) Acta Metall 20:735
3. Argon AS, Im J (1975) Metall Trans 6A:839
4. Rosselier G (1987) Nucl Eng Des 105:97
5. Gurson AL (1977) J Eng Mater Tech 99:2
6. Tvergaard V, Needleman A (1984) Acta Metall 32:157
7. Cheng, Yiu (1998) In: International Conference on non linear Mechanics, ICNM, pp 175–180
8. Decamp K, Bauvineau L, Besson J, Pineau A (1997) Int J Fracture 88:1
9. Ragab AR (2000) Int J Fract 105:391
10. Pineau A (1997) 14th Trans. 14th Int Conf Struct Mech SmiRt 14, Lyon, 1997
11. Lee JH, Zhang Y (1994) J Eng Mater Tech 116:69
12. Qiu YP, Weng GJ (1993) Int J Plast 6:271
13. Zhang ZL, Thaulow C, Ødegård J (2000) Eng Fract Mech 67(2):155
14. Rakin M, Cvijovic Z, Grabulov V, Putic S (2004) Eng Fract Mech 71(4–6):813
15. Pavankumar TV, Samal MK, Chattopadhyay J, Dutta BK, Kushwaha HS, Roos E, Seidenfuss M (2005) Int J Pressure Vessels Piping 82(5):386
16. Mkaddem A, Hambli R, Potiron A (2004) Int J Adv Manuf Tech 23:451
17. Qian XD, Choo YS, Liew JYR, Wardenier J (2005) J Struct Eng 131:768
18. Teng X, Wierzbick T, Hiermaier S, Rohr I (2005) Int J Struct Sol 42:2929
19. Chu C, Needleman A (1980) J Eng Mater Tech 102:249
20. Batoz JL, Dhatt G (1979) Int J Num Meth Eng 14:1262
21. Crisfield MA (1987) In: Owen DR, Hinton E, Onate E (eds) Computational plasticity Part-I. Pineridge Press, pp 133–159
22. Bathe KJ (1997) Finite element procedures. Printice Hall of India
23. Chattopadhyay J, Dutta BK, Kushwaha HS (2000) Int J Pressure Vessels Piping 77:455
24. Thomason PF (1990) Acta Metall 33:1079
25. Zahoor A (1992) Int J Pressure Vessels Piping 51:1